Power Electronic Systems
Laboratory

IEEE Transactions on Magnetics, Vol. 52, No. 7, July 2016

Angle-Sensorless Zero- and Low-Speed Control of Bearingless Machines

T. Wellerdieck,
T. Nussbaumer,
J. W. Kolar

Eidgenössische Technische Hochschule Zürich
Swiss Federal Institute of Technology Zurich

Angle-Sensorless Zero- and Low-Speed Control of Bearingless Machines

Tobias Wellerdieck[1], Thomas Nussbaumer[2], and Johann W. Kolar[1]

[1]Power Electronic Systems Laboratory, ETH Zürich, Zürich 8092, Switzerland
[2]Levitronix GmbH, Zürich 8005, Switzerland

Bearingless machines are successfully used for a variety of applications that demand for low mechanical losses, low wear, and low contamination. These machines require exact knowledge of the radial and angular rotor position in order to ensure stable levitation. This information is obtained with different position sensors. Alternatively, a sensorless approach can be used to determine the rotor position. The omission of the angular sensors leads to a reduction in costs and an improvement in reliability and allows to explore new areas of applications for bearingless machines. However, few zero and low-speed sensorless angle estimators are published to this date. Therefore, a novel model-based estimator to determine the rotor angle at zero and at low speeds and, thus, to allow sensorless operation over the whole speed range of the bearingless permanent magnet synchronous machine is proposed in this paper. The observer utilizes the radial position measurements and a model of the bearing force generation to determine the error of the angular position estimation. The method is implemented on a bearingless machine prototype, and the functionality is shown by measurements.

***Index Terms*—Bearingless, control, observer, sensorless.**

I. Introduction

A BEARINGLESS machine is an electric motor with an integrated magnetic bearing. The rotor of such a machine is levitated using a magnetic field. This eliminates the need for mechanical bearings and allows the rotor to be operated in a sealed compartment. Bearingless machines are well suited for applications with demands on high speeds, low wear, and low particle generation and contamination [1]–[3].

This paper focuses on a bearingless permanent magnet disk drive [4]. The rotor consists of a ring-shaped permanent magnet with a diameter that exceeds its axial length. This topology is advantageous, because it features passive stability in three degrees of freedom. Therefore, only three degrees of freedom have to be controlled actively [5], [6]. Fig. 1 shows a bearingless machine that utilizes such a topology and is used to verify the angle estimation method. The control system utilizes information from displacement and angular sensors to achieve stable levitation and a high drive performance. The cost and the complexity of the system can be reduced if an angle-sensorless control is used. This allows for new areas of operation for bearingless machines.

Different ways of sensorless estimation of the rotor angle for permanent magnet machines are reported in the literature [7]–[10]. These methods can be divided into two categories: either the machine voltages and currents are measured to obtain information about the induced voltage and the rotor flux angle or high-frequency signals are injected into the machine terminals to measure the phase inductances. The first approach requires a minimal amplitude of the induced voltage and, thus, can only be employed for medium and high speeds. The second approach works for all speed ranges. However, any rotor displacement in a bearingless machine will disturb the inductance measurement and, therefore, have a direct impact on the angle estimation.

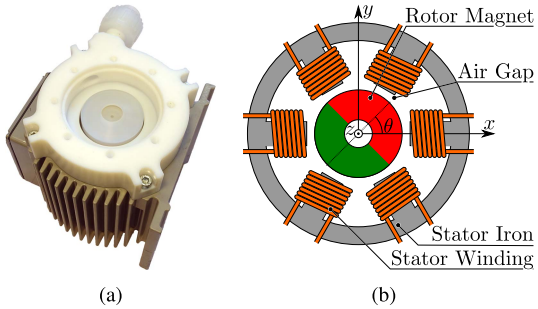

Fig. 1. (a) Picture of a bearingless permanent magnet machine prototype. (b) Schematic representation.

A feed-forward control method for operating bearingless machines at low speeds was introduced in [11]. The method utilizes dc to achieve passive angular stability of the rotor, leading to a low efficiency of the machine.

This paper proposes the usage of a novel, model-based zero- and low-speed-angle observer to obtain the rotor angle based on the observations of the radial bearing behavior. The force and the torque generation in a bearingless machine are described based on the flux density harmonics in the air gap. Subsequently, the influence of a rotor angle estimation error on the behavior of the radial position control is examined. This serves as a basis for the formulation of the angle observer structure. The operational principle of the observer is investigated through simulations, and the functionality of the method is shown by experiment.

II. Force and Torque Calculation

The radial forces and the torque acting upon the rotor of a bearingless machine can be calculated using the

Manuscript received November 6, 2015; revised January 8, 2016 and February 2, 2016; accepted February 3, 2016. Date of publication February 8, 2016; date of current version June 22, 2016. Corresponding author: T. Wellerdieck (e-mail: wellerdieck@lem.ee.ethz.ch).

Color versions of one or more of the figures in this paper are available online at http://ieeexplore.ieee.org.

Digital Object Identifier 10.1109/TMAG.2016.2527059

TABLE I
RELEVANT VARIABLES DEFINING THE MAGNETIC FLUX DENSITY IN THE AIR GAP OF A BEARINGLESS MACHINE

Description	Var.	Range
Displ. in x Direction	Δx	$\Delta x \in [-2\text{ mm}, 2\text{ mm}]$
Displ. in y Direction	Δy	$\Delta y \in [-2\text{ mm}, 2\text{ mm}]$
Rotor Angle	θ	$\theta \in [0, 2\pi]$
Drive Current	$\hat{I}_\mathrm{D}, \phi_\mathrm{D}$	$\hat{I}_\mathrm{D} \in [0, 5\text{ A}], \phi_\mathrm{D} \in [0, 2\pi]$
Bearing Current	$\hat{I}_\mathrm{B}, \phi_\mathrm{B}$	$\hat{I}_\mathrm{B} \in [0, 5\text{ A}], \phi_\mathrm{B} \in [0, 2\pi]$

TABLE II
RELEVANT FIELD HARMONICS OF THE RADIAL AND TANGENTIAL FLUX DENSITY COMPONENTS IN THE AIR GAP ($k \in [r, t]$)

Description	Amplitude	Relevant Harmonics
Zero Displacement	$\hat{B}_{\mathrm{k,i},0} = \text{const}$	$i \in [1, 3, 5, 7]$
Rotor Displacmenet	$\hat{B}_{\mathrm{k,i},\Delta} \propto \sqrt{\Delta x^2 + \Delta y^2}$	$i \in [2, 4, 6, 8]$
Bearing Field	$\hat{B}_{\mathrm{k,i,B}} \propto \hat{I}_\mathrm{B}$	$i \in [2, 4, 8]$
Drive Field	$\hat{B}_{\mathrm{k,i,D}} \propto \hat{I}_\mathrm{D}$	$i \in [1, 5, 7]$

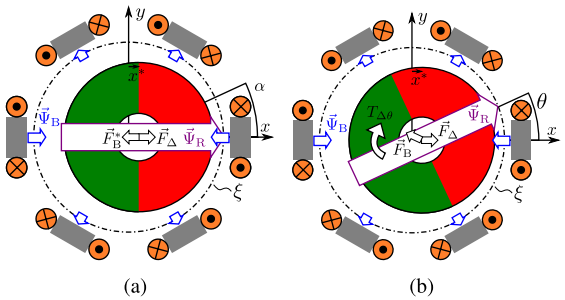

Fig. 2. Passive and bearing forces for a displaced rotor with (a) zero angle estimation error and (b) non-zero angle estimation error.

Maxwell stress tensor [12]. The force and the torque calculation neglects z components of the flux due to the axial symmetry of the bearingless disk drive. Therefore, it is sufficient to consider the radial and tangential flux components in the air gap. The calculation is carried out by integrating along the contour ξ shown in Fig. 2. The coordinate α depicts the position on ξ. Force and torque are calculated as

$$\begin{aligned} F_\mathrm{x} &\propto \int_0^{2\pi} \left(B_\mathrm{r}^2 - B_\mathrm{t}^2\right)\cos(\alpha) - (2B_\mathrm{t}B_\mathrm{r})\sin(\alpha)d\alpha \\ F_\mathrm{y} &\propto \int_0^{2\pi} \left(B_\mathrm{r}^2 - B_\mathrm{t}^2\right)\sin(\alpha) + (2B_\mathrm{t}B_\mathrm{r})\cos(\alpha)d\alpha \\ T_\mathrm{z} &\propto \int_0^{2\pi} B_\mathrm{t}B_\mathrm{r}d\alpha. \end{aligned} \tag{1}$$

The flux density components B_r and B_t can be approximated by their space harmonics $B_{\mathrm{k,i}}$ as

$$B_\mathrm{k}(\alpha) \approx \sum_i \hat{B}_{\mathrm{k,i}} \sin(i\alpha + \phi_{\mathrm{k,i}}), \quad k \in [r, t]. \tag{2}$$

The amplitude $\hat{B}_{\mathrm{k,i}}$ and the phase $\phi_{\mathrm{k,i}}$ of the space harmonics are dependent on the rotor position as well as the drive and bearing currents in the stator windings.

If magnetic saturation is neglected, then the ith space harmonic of the magnetic flux density can be stated as

$$\begin{aligned} B_{\mathrm{k,i}} = {} & B_{\mathrm{k,i},0}(\theta) + B_{\mathrm{k,i},\Delta}(\theta, \Delta x, \Delta y) \\ & + B_{\mathrm{k,i,B}}(\hat{I}_\mathrm{B}, \phi_\mathrm{B}) + B_{\mathrm{k,i,D}}(\hat{I}_\mathrm{D}, \phi_\mathrm{D}) \end{aligned} \tag{3}$$

with the relevant variables listed in Table I. Table II lists the correlations between the parameters and the harmonics, where $\hat{I}$ is the amplitude and ϕ is the phase of a current.

III. BEARING BEHAVIOR

The radial position controller of a bearingless machine controls the bearing currents in the stator windings to ensure a stable levitation of the rotor at a given reference position x^* and y^*. The controller requires information about the radial position and the angle of the rotor magnet to achieve this task. It is assumed that the radial position is known exactly, but the rotor angle is only estimated. The actual rotor angle is denoted by θ, the estimation is denoted by $\hat{\theta}$, and the error is denoted by $\Delta\theta = \hat{\theta} - \theta$.

Assume that $\theta = 0$, meaning that the rotor flux $\vec{\Psi}_\mathrm{R}$ is placed on the x-axis, there is no angle estimation error, $\hat{\theta} = \theta$, and the rotor is at a reference rotor position $x^* > 0$, $y = 0$, as shown in Fig. 2(a). If higher flux density harmonics are neglected, the flux density components on the contour ξ are

$$\begin{aligned} B_{\mathrm{r},1} &= \hat{B}_{\mathrm{r},1,0}\cos(\alpha) \\ B_{\mathrm{t},1} &= \hat{B}_{\mathrm{r},1,0}\cos(\alpha - \pi/2) \\ B_{\mathrm{r},2} &= \hat{B}_{\mathrm{r},2,\Delta}\cos(2\alpha) \\ B_{\mathrm{t},2} &= \hat{B}_{\mathrm{t},2,\Delta}\cos(2\alpha - \pi/2) \end{aligned} \tag{4}$$

with $\hat{B}_{\mathrm{r},2} > \hat{B}_{\mathrm{t},2}$. Inserting (4) into (1) shows that the radial displacement results in a force $\vec{F}_\Delta$. The bearing controller needs to generate a bearing force $\vec{F}_\mathrm{B}^*$ that compensates $\vec{F}_\Delta$. Therefore, the radial position controller imposes bearing currents in the stator coils leading to the bearing flux density harmonics

$$\begin{aligned} B_{\mathrm{r},2,\mathrm{B}} &= \hat{B}_{\mathrm{r},2,\mathrm{B}}\cos(2\alpha + \pi) \\ B_{\mathrm{t},2,\mathrm{B}} &= \hat{B}_{\mathrm{t},2,\Delta}\cos(2\alpha + \pi/2) \end{aligned} \tag{5}$$

which, according to (1), leads to a zero net force and zero torque.

However, if the rotor angle estimate is not correct, then the bearing will behave differently. Assuming that the rotor angle is changed to $\theta > 0$, as shown in Fig. 2(b). The passive flux density harmonics of order one and two are

$$\begin{aligned} B_{\mathrm{r},1,0} &= \hat{B}_{\mathrm{r},1}\cos(\alpha - \theta) \\ B_{\mathrm{t},1,0} &= \hat{B}_{\mathrm{r},1}\cos(\alpha - \theta - \pi/2) \\ B_{\mathrm{r},2} &= \hat{B}_{\mathrm{r},2,\Delta}\cos(2\alpha - \theta) \\ B_{\mathrm{t},2} &= \hat{B}_{\mathrm{t},2,\Delta}\cos(2\alpha - \theta - \pi/2). \end{aligned} \tag{6}$$

Assume that the radial position controller has no information about the new rotor angle, meaning that the estimated angle $\hat{\theta} = 0 \Leftrightarrow \Delta\theta > 0$. Therefore, the bearing flux components are as given in (5). Inserting (5) and (6) into (1) results in

$$F_{\mathrm{B,x}} < F_{\mathrm{B,x}}^*, \quad F_{\mathrm{B,y}} > F_{\mathrm{B,y}}^* = 0, \quad T_\mathrm{z} < 0. \tag{7}$$

This shows that a rotor angle estimation error $|\Delta|\theta > 0$ has two effects on the bearing behavior. First, the second-order flux harmonics of a displaced rotor and the bearing harmonics lead to a torque $T_{\Delta,\mathrm{z}}$. The magnitude of this torque is proportional to the displacement. The torque is forcing the rotor angle to the estimated angle, and driving the estimation error $\hat{\theta}$ to zero.

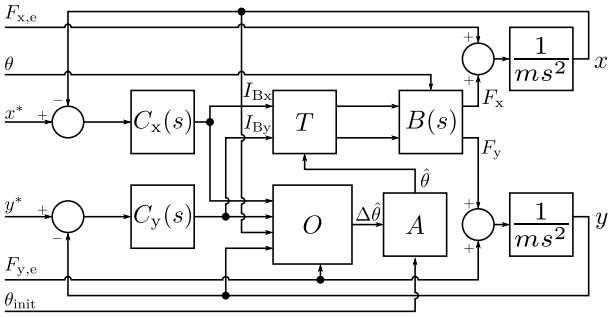

Fig. 3. Simplified block diagram of the radial bearing and the angle observer.

Second, the angle estimation error leads to a deviation of the bearing force. The applied bearing forces $\vec{F}_B$ can be stated depending on the ideal bearing forces $\vec{F}_B^*$ and the rotor angle estimation error as

$$\vec{F}_{\mathrm{B}} = \begin{bmatrix} \cos(\Delta\theta) & -\sin(\Delta\theta) \\ -\sin(\Delta\theta) & \cos(\Delta\theta) \end{bmatrix} \cdot \vec{F}_{\mathrm{B}}^*. \tag{8}$$

IV. Observer Structure

The angle observer is based on the force coupling described in (8). The observer estimates the angle error $\Delta\hat{\theta}$ by evaluating the difference between the ideal bearing force $\vec{F}_{\mathrm{B}}^*$ and the actual bearing force $\vec{F}_{\mathrm{B}}$.

A simplified block diagram of the radial bearing with observer is shown in Fig. 3. The two position controllers are labeled $C_{\mathrm{x}}(s)$ and $C_{\mathrm{y}}(s)$ and are of a PID structure. The radial bearing is labeled $B(s)$, and the estimation error observer is labeled O. The estimated rotor angle is adapted in the block A. The position controllers calculate the reference bearing currents I_{Bx} and I_{By} based on the deviation of the rotor position x, y from the reference position x^*, y^*. Block T denotes a park transformation, transforming the bearing currents from the rotor flux orientated coordinate system to the stator orientated coordinate system by rotating them with the angle $\hat{\theta}_{\mathrm{R}}$. The transformed currents will lead to the forces F_{x} and F_{y}, according to (1), which define the rotor movement together with any external forces $F_{\mathrm{x,e}}$ and $F_{\mathrm{y,e}}$. The external forces consist of the displacement force and possible disturbance forces.

The observer block O calculates an estimate of the rotor angle error

$$\Delta\hat{\theta} = \angle(\vec{I}_{\mathrm{B}}) - \angle(\vec{F}_{\mathrm{r,e}}) - 180° \tag{9}$$

as the difference between the angle of the bearing current $\vec{I}_B$ and the angle of an external radial force $\vec{F}_{r,e}$. This force can be the gravitational force or a displacement force, as shown in Fig. 2. The implementation of O is depending on the presence or absence of radial gravitational pull. If the external force is created by rotor displacement, then the direction of the force can be calculated as

$$\angle\vec{F}_{\mathrm{r,e}} = \angle\vec{r} = \arctan\left(\frac{y}{x}\right). \tag{10}$$

Therefore, the angle estimation error $\Delta\hat{\theta}$ can be calculated using $\vec{I}_{\mathrm{B}}$ and the rotor position x and y. Block A calculates $\hat{\theta}$ based on θ_{init} and $\Delta\hat{\theta}$ as

$$\hat{\theta}(t) = \theta_{\mathrm{init}} + P_{\mathrm{obs}} \cdot \Delta\hat{\theta}(t) + I_{\mathrm{i}} \cdot \int_0^t \Delta\hat{\theta}(\tau)d\tau \tag{11}$$

where P_{A} and I_{A} are the proportional and integrator gain of the adaption mechanism.

The functionality of the observer block O can be illustrated with the following example. Assume that the rotor is levitating, the rotor angle is known, i.e., $\Delta\theta = \hat{\theta} - \theta = 0$, and an external radial force $\vec{F}_{\mathrm{r,e}}$ is applied. The net force acting on the rotor is zero in stable levitation. Therefore, the bearing force $\vec{F}_{\mathrm{B}}$ is pointing in the opposite direction of $\vec{F}_{\mathrm{r,e}}$. Inserting $\Delta\theta = 0$ into (8) shows that $\vec{F}_B^*$ and $\vec{I}_{\mathrm{B}}$ are parallel to $\vec{F}_{\mathrm{B}}$, and note that k_{B} is the bearing force constant. The corresponding pointer diagram is shown in Fig. 4(a). Fig. 4(b) shows the same example with an angle estimation error $\Delta\theta \neq 0$. The net force acting upon the rotor is still zero, and therefore, $\vec{F}_{\mathrm{B}}$ is opposing $\vec{F}_{\mathrm{r,e}}$. However, F_{B}^* and subsequently $\vec{I}_{\mathrm{B}}$ are rotated by $\Delta\theta$ according to (8). The angle observer detects that the angle between $\vec{F}_{\mathrm{r,e}}$ and $\vec{I}_{\mathrm{B}}$ is no longer 180° and corrects the angle estimate $\hat{\theta}$ to drive $\Delta\theta$ to zero.

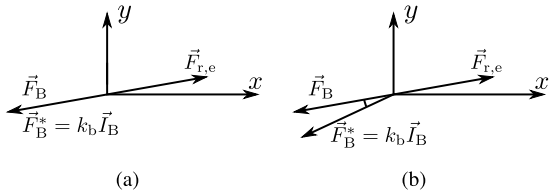

Fig. 4. Pointer diagram showing the forces acting on a rotor in stable levitation with (a) no estimation error and (b) non-zero estimation error.

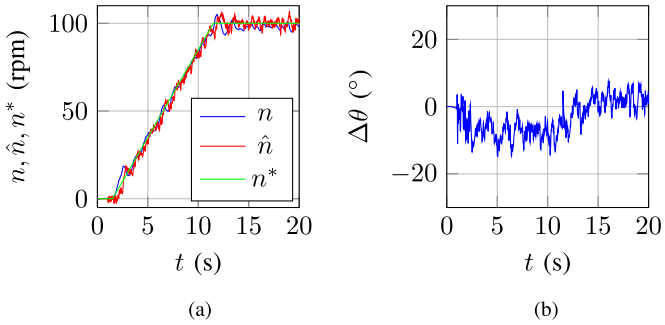

Fig. 5. Simulation of closed-loop observer performance for (a) acceleration from 0 to 100 r/min showing the rotor speed and rotor speed estimate and (b) estimation error.

The net force acting on the rotor is zero in stable levitation. Therefore, the bearing force $\vec{F}_{\mathrm{B}}$ is pointing in the opposite direction of $\vec{F}_{\mathrm{r,e}}$. Inserting $\Delta\theta = 0$ into (8) shows that $\vec{F}_B^*$ and $\vec{I}_{\mathrm{B}}$ are parallel to $\vec{F}_{\mathrm{B}}$, and note that k_{B} is the bearing force constant. The corresponding pointer diagram is shown in Fig. 4(a). Fig. 4(b) shows the same example with an angle estimation error $\Delta\theta \neq 0$. The net force acting upon the rotor is still zero, and therefore, $\vec{F}_{\mathrm{B}}$ is opposing $\vec{F}_{\mathrm{r,e}}$. However, F_{B}^* and subsequently $\vec{I}_{\mathrm{B}}$ are rotated by $\Delta\theta$ according to (8). The angle observer detects that the angle between $\vec{F}_{\mathrm{r,e}}$ and $\vec{I}_{\mathrm{B}}$ is no longer 180° and corrects the angle estimate $\hat{\theta}$ to drive $\Delta\theta$ to zero.

Fig. 5 shows a simulation of the operation of a bearingless machine operated with the angle estimator. The simulation models the machine shown in Fig. 1 and captures its dynamics by including all flux density harmonics listed in Table II. Furthermore, non-idealities, such as measurement noise, are also modeled. The simulation assumes that there is no radial gravitational pull, and therefore, the radial reference position is set to

$$r^* = \sqrt{(x^*)^2 + (y^*)^2} > 0. \tag{12}$$

This results in a radial displacement force $\vec{F}_\Delta$ according to (1) that must be overcome by the bearing. The displacement

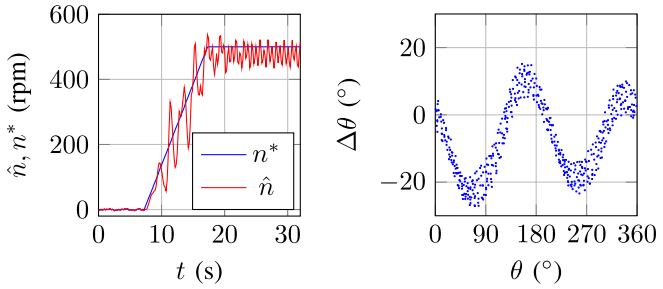

Fig. 6. Logged data from the control of the test machine showing the machine speed for (a) acceleration from 0 to 500 r/min and (b) difference between estimated and measured angle at 500 r/min.

force is used as $\vec{F}_{\mathrm{r,e}}$ in (9) to determine the rotor angle. The simulation is initialized with the correct rotor angle, i.e., $\Delta\theta = 0$. The estimated angle error $\Delta\hat{\theta}$ is calculated according to (9). The integrator in (11) drives the estimation error $\Delta\theta$ to zero once the rotor speed reaches the reference speed [see Fig. 5(b)].

The estimation error is shown in Fig. 5(b). The rotor speed estimate is calculated by the derivation of the angle estimate and is used for the drive current controller. Fig. 5(a) shows the machine speed n, the reference speed n^*, and the machine speed estimate $\hat{n}$. The machine speed is constant after approximately 11 s.

V. Implementation

The angle estimation method has been implemented on a commercially available machine [see Fig. 1(a)] to verify the functionality of the model-based angle estimation. The control utilizes only the estimated angle for operation, and angle sensors are used to calculate the estimation error. The machine speed is obtained by taking the time derivative of the estimated angle.

The angle-sensorless initial angle detection and start-up procedure are taken from [11]. The novel angle estimation method is started once the rotor reached stable levitation. The rotor reference position was displaced to generate a sufficient external radial force.

The machine was successfully operated up to rotating speeds of 500 r/min, which is sufficient to switch to an observer method relying on the induced voltage. The plots in Fig. 6 show logged data values from the control. It is assumed that the angle sensors measure the rotor angle with negligible error, i.e., $\theta_{\mathrm{measured}} = \theta$. Fig. 6(a) shows the reference and estimated speed for an acceleration from 0 to 500 r/min. The angle estimation error $\Delta\theta$ for a constant machine speed of 500 r/min is shown in Fig. 6(b). The machine efficiency at 500 r/min is increased by ∼20% compared with the efficiency with feed-forward control proposed in [11].

The observer method works as long as radial disturbance forces acting upon the rotor are small compared with the displacement force, which is applied by the observer algorithm.

Any unknown radial disturbance force $\vec{F}_\delta$ will lead to an angle estimation error $\Delta\hat{\theta}_\delta$ that cannot be detected by the angle estimator.

Radial disturbance forces, as they can be observed, e.g., in hydraulic machines, such as blowers or pumps, are highly speed dependent and are generally very low in the observer speed range. Known static forces, such as the gravitational force or static pressure, can be actively compensated for.

Furthermore, any error in the current or position measurement will have a direct impact on the quality of the estimation. This is most likely the reason for the non-zero mean value of the angle estimation error at 500 r/min.

Radial disturbance forces, as they can be observed, e.g., in hydraulic machines, such as blowers or pumps, are highly speed dependent and are very low in the speed range of the observer.

VI. Conclusion

The angle observer structure proposed in this paper allows the estimation of the rotor angle for zero and low speeds. A proof of concept is shown for low speeds using a commercially available machine.

Further improvement of the performance of the method is possible by the optimization of the observer, the position, and the speed controllers. This requires a more detailed analysis of non-ideal effects in the bearing and a formulation of the dynamics of the complete control system.

Acknowledgment

This work was supported by the Swiss Commission for Technology and Innovation.

References

[1] A. O. Salazar, A. Chiba, and T. Fukao, "A review of developments in bearingless motors," in *Proc. 7th Int. Symp. Magn. Bearings*, May 2000, pp. 335–340.

[2] J. Amemiya, A. Chiba, D. G. Dorrell, and T. Fukao, "Basic characteristics of a consequent-pole-type bearingless motor," *IEEE Trans. Magn.*, vol. 41, no. 1, pp. 82–89, Jan. 2005.

[3] T. Tezuka, N. Kurita, and T. Ishikawa, "Design and simulation of a five degrees of freedom active control magnetic levitated motor," *IEEE Trans. Magn.*, vol. 49, no. 5, pp. 2257–2262, May 2013.

[4] X. Sun, L. Chen, and Z. Yang, "Overview of bearingless permanent-magnet synchronous motors," *IEEE Trans. Ind. Electron.*, vol. 60, no. 12, pp. 5528–5538, Dec. 2013.

[5] W. Gruber, S. Silber, W. Amrhein, and T. Nussbaumer, "Design variants of the bearingless segment motor," in *Proc. Int. Symp. Power Electron. Elect. Drives Autom. Motion (SPEEDAM)*, Jun. 2010, pp. 1448–1453.

[6] T. Nussbaumer, P. Karutz, F. Zurcher, and J. W. Kolar, "Magnetically levitated slice motors—An overview," *IEEE Trans. Ind. Electron.*, vol. 47, no. 2, pp. 754–766, Mar. 2011.

[7] J.-S. Kim and S.-K. Sul, "New approach for high-performance PMSM drives without rotational position sensors," *IEEE Trans. Power Electron.*, vol. 12, no. 5, pp. 904–911, Sep. 1997.

[8] H.-W. Park, S.-H. Lee, T.-H. Won, M.-S. Kim, and C.-U. Kim, "Position sensorless speed control scheme for permanent magnet synchronous motor drives," in *Proc. IEEE Int. Symp. Ind. Electron. (ISIE)*, vol. 1. Jun. 2001, pp. 632–636.

[9] P. P. Acarnley and J. F. Watson, "Review of position-sensorless operation of brushless permanent-magnet machines," *IEEE Trans. Ind. Electron.*, vol. 53, no. 2, pp. 352–362, Apr. 2006.

[10] S.-Y. Kim and I.-J. Ha, "A new observer design method for HF signal injection sensorless control of IPMSMs," *IEEE Trans. Ind. Electron.*, vol. 55, no. 6, pp. 2525–2529, Jun. 2008.

[11] K. Raggl, B. Warberger, T. Nussbaumer, S. Burger, and J. W. Kolar, "Robust angle-sensorless control of a PMSM bearingless pump," *IEEE Trans. Ind. Electron.*, vol. 56, no. 6, pp. 2076–2085, Jun. 2009.

[12] K. J. Meessen, J. J. H. Paulides, and E. A. Lomonova, "Force calculations in 3-D cylindrical structures using Fourier analysis and the Maxwell stress tensor," *IEEE Trans. Magn.*, vol. 49, no. 1, pp. 536–545, Jan. 2013.